minerals

MDPI

Article

Developed Recyclable CaFe-Layered Double Hydroxide for Efficient Cadmium Immobilization in Soil: Performance and Bioavailability

Yuqi Jing [1], Ran Chen [1], Jiayao Zhang [1], Liyun Hu [1] and Xinhong Qiu [1,2,3,*]

[1] School of Chemistry and Environmental Engineering, Wuhan Institute of Technology, Wuhan 430205, China; 18907282014@163.com (Y.J.); ranchen266@gmail.com (R.C.); jiayaozhang667@gmail.com (J.Z.)
[2] Key Laboratory of Novel Biomass-Based Environmental and Energy Materials in Petroleum and Chemical Industry, Wuhan 430074, China
[3] Wuhan Institute of Technology Jingmen Research Institute of New Chemical Materials Industry Technology, Wuhan 430070, China
* Correspondence: qxinhong@gmail.com or qiuxh@wit.edu.cn; Tel./Fax: +86-27-8719-5680

Abstract: Powdered layered double hydroxide (CaFe-LDH) was synthesized via hydrothermal co-precipitation, demonstrating successful preparation upon characterization. Subsequently, experiments were conducted to assess its efficacy in immobilizing divalent cadmium (Cd(II)). The findings substantiated the effectiveness of CaFe-LDH in immobilizing Cd(II) within soil. Various influencing factors, including LDH dosage, pH, and soil heavy metal concentration, were systematically investigated, revealing CaFe-LDH's superiority in Cd(II) immobilization. Notably, the leaching concentration of Cd(II) was notably reduced from 142.30 mg/L to 32.99 mg/L, with a maximum adsorption capacity of 31.10 mg/L, underscoring the significant role of CaFe-LDH in Cd(II) removal. Furthermore, the stability of CaFe-LDH was confirmed via toxicity characteristic leaching procedure (TCLP) experiments and plant potting tests. In-depth analysis of the immobilization mechanism through X-ray diffraction (XRD), X-ray photoelectron spectroscopy (XPS), Fourier-transform infrared spectroscopy (FTIR), energy-dispersive X-ray spectroscopy (EDS), and scanning electron microscopy (SEM) elucidated isomorphous substitution and surface adsorption as the primary mechanisms responsible for Cd(II) immobilization in contaminated soils. Additionally, isomorphic substitution and adsorption onto oxygen-containing functional groups were observed. This comprehensive study underscores the promising potential of CaFe-LDH in immobilizing Cd(II) in contaminated soil. With its commendable immobilization properties and recyclability, CaFe-LDH emerges as a promising solution for remediating heavy-metal-contaminated soils.

Keywords: CaFe-LDH; Cd(II) immobilization; magnetic recovery; phytoremediation

Citation: Jing, Y.; Chen, R.; Zhang, J.; Hu, L.; Qiu, X. Developed Recyclable CaFe-Layered Double Hydroxide for Efficient Cadmium Immobilization in Soil: Performance and Bioavailability. *Minerals* **2024**, *14*, 656. https://doi.org/10.3390/min14070656

Academic Editor: Manuel Pozo Rodríguez

Received: 16 April 2024
Revised: 20 June 2024
Accepted: 24 June 2024
Published: 26 June 2024

1. Introduction

In contemporary societies, the acceleration of soil and environmental pollution by heavy metals is a consequence of industrialization, rapid population growth, and intensified agriculture, leading to the accumulation of heavy metals. This accumulation often results in soil and water degradation, as well as ecosystem dysfunction. Additionally, heavy metals have infiltrated the food chain from contaminated sources, including soil, water, and air, posing a significant threat to human and animal health [1]. The issue of soil–heavy-metal pollution, notably cadmium (Cd) pollution, has become increasingly severe. Cd pollution ranks foremost, with a point exceedance rate as high as 7.0%. Soil Cd's bioeffectiveness is notably heightened under low pH conditions, presenting health and safety risks to agricultural produce, such as elevated Cd levels in rice [2]. Concurrently, as a consequence of accelerated industrialization, certain industrial and ore mining operations are leading to the infiltration of heavy metals into floodplains, along with river water and sediments [3].

Given the profound interplay between soil and the aquatic environment, floodplain soils can be perceived as semi-terrestrial, with either waterlogged or shallow water conditions, harboring distinctive ecosystems. Additionally, owing to their naturally high fertility, many floodplain soils have been extensively utilized for agricultural and reforestation purposes for extended periods [4]. The potential entry of toxic metals into these floodplains poses a significant threat to the ecosystem, food chain, and, ultimately, soil and human health [5]. At present, a staggering 5 million sites spanning 500 million hectares worldwide are suffering from soil contamination, primarily due to the presence of various heavy metals or metalloids with concentrations surpassing geographical baselines and regulatory thresholds [6]. The cumulative economic impact of this soil–heavy-metal contamination on the global economy is projected to exceed a colossal USD 10 billion annually [7]. In China, the standard for Cd content in agricultural land is set at 0.3 $mg \cdot kg^{-1}$ of total cadmium (or 0.6 $mg \cdot kg^{-1}$ for pH > 7.5) [8]. Cd primarily exists in soil in various forms, including $CdCl_2$, $Cd(NO_3)_2$, $Cd(PO_4)_2$, $CdCO_3$, among others [9].

Current methods for remediating heavy-metal-contaminated soil encompass electrokinetic soil remediation technology, chemical leaching technology, phytoremediation, microbial remediation, and combined remediation approaches [10]. In regard to adsorption as one of the effective methods for treating heavy metals, a study has successfully synthesized a new type of magnesium–aluminum metal oxide using materials that can be deposited on a template. The Mg-Al metal oxide composites were synthesized by filter paper templates under hydrothermal conditions, and layered porous materials were obtained. The new composite material is more effective in adsorbing SL from oilfield wastewater and is an efficient high-performance material for wastewater treatment [11]. However, its scalability is hindered by high operational costs, time consumption, and adverse modifications to soil physicochemical properties crucial for crop growth [12,13]. In contrast, passivation has emerged as an effective technique in treating heavy-metal-contaminated soils. Anionic clay minerals, among other passivators, offer advantages in terms of cost-effectiveness and environmental treatment efficiency. Many mineral materials show good adsorption effects, such as montmorillonite, which has vertical expandability and a large internal and external surface area, and therefore has a certain adsorption capacity [14]; additionally, kaolinite has a relatively low cation exchange capacity and small surface area, which is more effective for the removal of heavy metals [15]. LDH (layered double hydroxide) has been extensively studied for its high efficiency in immobilizing Cd(II) during soil remediation. For instance, Kong et al. demonstrated that CaAl-LDH efficiently traps Cd^{2+} cations, leading to their immobilization in the resultant CdAl-LDH structure [16]. Elham et al. explored the exchange of sulfide-based materials with LDH counter-anion interlayers, resulting in well-coordinated dentate structures capable of adsorbing soft heavy metals [17]. Where carbonate-inserted hydrotalcites such as Mg-Al-CO_3-LDH clearly exhibit adsorption capacities similar to or superior to other adsorbent materials, Cd(II) ions make contact with charge-compensated carbonate ions attached to the surface and edges to form $CdCO_3$ precipitates, thus removing Cd [18].

However, irrespective of the passivator used for soil remediation, residues remain in the soil, exerting uncontrolled environmental effects [19]. Particularly, inorganic passivators, often applied in large quantities (around 5%), can adversely impact soil physicochemical properties and bacterial metabolism, posing further environmental sensitivity concerns [20,21]. Moreover, passivator residues represent a wastage of resources [22]. Current research primarily focuses on the efficacy of passivators in enriching heavy metals in soil while neglecting their recycling and reuse.

Therefore, developing an effective process for passivator recovery is imperative. Magnetic recycling serves as a widely adopted method due to its efficiency, operational simplicity, and low equipment costs [23]. While previous studies, such as Li et al.'s synthesis of LDHs-M microspheres encapsulated in magnetic iron within calcium alginate, demonstrated promising recoverability, encapsulation led to a structurally complex material with a reduced specific surface area and exposure, consequently compromising reaction charac-

teristics [24]. This study aims to employ a simpler, exposed, non-encapsulated material for Cd-contaminated soil remediation. Therefore, CaFe-LDH, characterized by its magnetic properties [25], is proposed for direct utilization in Cd soil solidification [26], offering the advantage of direct recyclability owing to its magnetic properties.

This study utilizes CaFe-LDH with magnetic properties for remediating Cd(II)-contaminated soil, which is subsequently recovered in an electrolyte solution using a conveyor belt under an external magnetic field for regeneration and recycling back to Cd(II)-contaminated soil. A series of experiments are conducted to assess CaFe-LDH's immobilization capacity under various influencing factors (e.g., reaction time, initial concentration, soil pH, dosage). The problem of small specific surface areas due to the use of encapsulated materials, such as sodium alginate, in other studies from the literature is solved, while the magnetic properties of iron oxide are utilized to achieve recycling and to reduce the secondary contamination of soil by residual LDH in the soil. Magnetic recovery, regeneration, and reuse of magnetic beads in real conveyor belt systems are explored to expand LDH recovery possibilities in engineering applications. Moreover, various characterizations are employed to elucidate the immobilization mechanism of CaFe-LDH for Cd(II) in soil. This study aims to enhance LDH recovery efficiency, improve soil remediation, and restore soil to its original state.

2. Materials and Methods

2.1. Synthesis of CaFe-LDH

In this experiment, CaFe-LDH was synthesized via the co-precipitation method. Specifically, 0.9446 g $Ca(NO_3)_2 \cdot 4H_2O$, 0.8080 g $Fe(NO_3)_3 \cdot 9H_2O$, and 0.5120 g NaOH were weighed and dissolved in 80 mL of solution at a Ca:Fe ratio of 2:1, respectively. The mixed aqueous solution was magnetically stirred for 30 minutes while maintaining the pH between 11.8 and 12.2. The well-mixed suspension was then transferred into a PTFE container and subjected to 120 °C for 48 h. Upon completion of the reaction, the mixture was cooled to room temperature, collected, washed, and centrifuged with deionized water. The resulting slurry was dried in an oven at 50 °C, milled, and labeled as CaFe-LDH [27,28].

2.2. Preparation of Test Soil

Soil samples were obtained from clean soil in Jiangsu Province, China. After preliminary removal of impurities, such as stones, the soil was air-dried, ground, and sieved through a 100-mesh sieve before use.

The procedure for preparing Cd(II)-containing test soil was as follows: Cadmium nitrate tetrahydrate was used to prepare a solution with a specific cadmium concentration, which was then mixed with clean soil samples at a solid–liquid ratio of 1 g−1 mL. The mixture was thoroughly stirred, air-dried, ground, and sealed for preservation. Additionally, different pH soil samples were prepared using 0.1 M HNO_3 and 0.1 M HCl for pH adjustment.

2.3. Experiments on the Solidification of Cd(II) in Soil

In centrifuge tubes, 1 g of Cd(II)-containing contaminated soil was weighed, followed by the addition of the required amount of CaFe-LDH for the experiment. Subsequently, 5 mL of ultrapure water was added to the mixture and homogenized at 30 rpm for a specific reaction time. After the reaction, the centrifuge tubes were centrifuged, and the supernatant was filtered. Next, 5.0 mL of 0.1 M $CaCl_2$ solution was added to the soil, and the mixture was allowed to react for 1 h before centrifugation [29]. The supernatant was then filtered using a 0.45 μm syringe, and the Cd(II) concentration was determined using an atomic absorption spectrophotometer.

The remaining residue in the centrifuge tubes was dried in an oven for subsequent toxicity entry, exit experiments, and soil analysis, with parallel samples being set up for consistency.

2.4. TCLP Soil Leaching Experiments

The potential environmental hazards of Cd(II)-contaminated soils were assessed using the standard toxicity characteristic leaching procedure (TCLP) recommended by USEPA Method 1311 [30]. The pH of the samples was determined initially, followed by loading 0.5 g of dried soil sample and 10 mL of extractant at a solid–liquid ratio of 20:1, L/kg into centrifuge tubes. The mixture was stirred at 30 ± 2 rpm and room temperature for 18 h. After the reaction, the supernatant was collected for analysis of Cd(II) leaching concentration in the solid waste.

2.5. Phytotoxicity Test

A batch of Petri dishes were prepared, with each containing 5 g of clean soil, Cd-contaminated soil, and CaFe-LDH remediation soil as parallel samples. Deionized water and 15 mung bean seeds were added to each dish, which were then cultivated at room temperature and watered daily. The growth conditions of mung bean seedlings were recorded over seven days, including measurements of the root, stem, and leaf lengths.

2.6. Determination of Cd Content in Plants

Mung bean seedlings after seven days of cultivation were cleaned with deionized water, and their roots, stems, and leaves were separated, dried and weighed. The dried roots, stems and leaves, were calcined in a muffle furnace at 550 °C for 6 h; then the ashes were transferred to a polytetrafluoroethylene reactor, to which 2 mL of HNO_3, 1 mL of H_2O_2 and 1 mL of deionized water were added, and the reactor was placed in an oven at 100 °C for 4 h. After the digestion was completed, the solution was filtered through a 0.45 μm membrane, and the Cd concentration was determined.

2.7. Extraction Experiment of Cd(II) in Soil

In this experiment, the water-leaching method, calcium-chloride-extraction method, and Tessier sequential extraction method were adopted to evaluate the different forms of Cd(II) in soil. The calcium-chloride-extraction method can effectively extract the concentration of Cd(II) in soil and determine the influence of environmental factors through the change of this concentration. The Tessier sequential extraction method can measure the content of exchangeable, carbonate-bound, Fe-Mn oxide-bound, organic-matter-bound, and residual state of Cd(II) in soil, which can be used to assess the changes of the morphology of Cd(II) before and after immobilization. The results were used to evaluate the changes of Cd(II) morphology in soil before and after solidification, which will be helpful for analyzing the passivation mechanism of CaFe-LDH.

2.8. Characterization and Morphology

The crystal structure of LDHs-M was determined using an X-ray diffractometer (XRD) (Bruker, Berlin, Germany) with Cu/Kα radiation (30 KV, 20 mA) at 0.02° steps. The functional groups of LDHs-M microspheres were detected by Fourier-transform infrared spectroscopy (FTIR) using a Nicolet-6700 (Thermo Electron, Waltham, MA, USA). A JSM-5510LV scanning electron microscope (SEM) (JEOL, Tokyo, Japan) with an energy-dispersive spectrometer (EDS) was used for accelerating voltages at 15 kV and 20 kV to The morphology of LDHs-M was obtained. The magnetization intensity of LDHs-M microspheres was recorded by a vibrating sample magnetometer (VSM) model 7404 (LakeShore, Carson, CA, USA). In addition, changes in elemental valence states were analyzed using an X-ray photoelectron spectrometer (Thermo Scientific K-Alpha).

3. Results and Discussion

3.1. Characterization of CaFe-LDH

Figure 1a illustrates the characteristic reflection of the LDH structure (PDF 48-0065) [31,32] in a CaFe-LDH–nitrate intercalation, evidenced by diffraction peaks at typical positions, namely (001), (002), and (110), approximately at 11.5°, 23.1°, and 29.8°, respectively. More-

over, characteristic diffraction peaks of the $Ca(OH)_2$ structure were detected at around 19.7°, 25.5°, and 34.3° [33]. From the XRD plots, we found that the solid is amorphous.

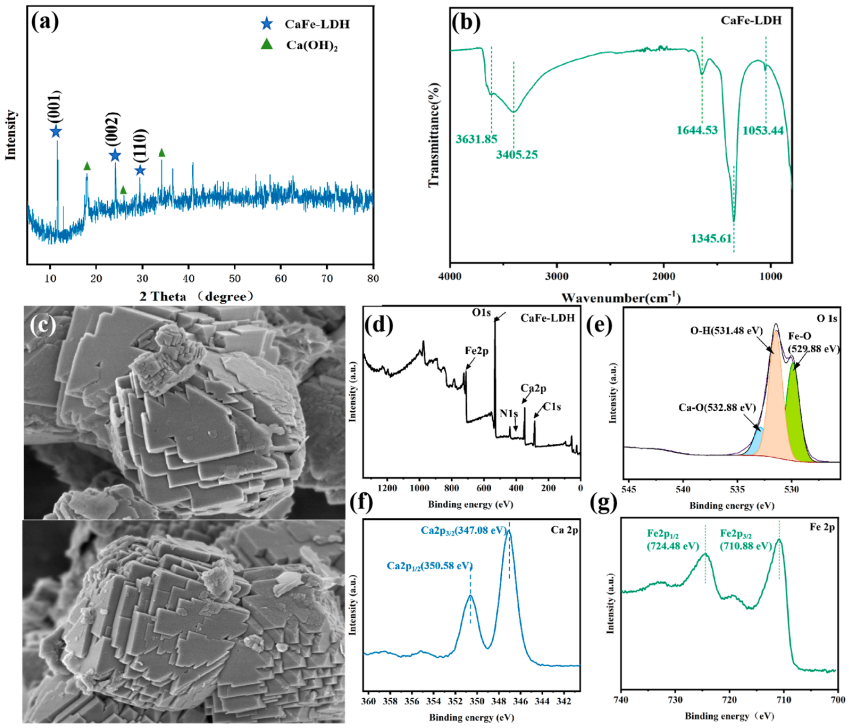

Figure 1. (**a**) XRD pattern of CaFe-LDH; (**b**) Fourier-transform infrared spectra of CaFe-LDH; (**c**) scanning electron microscopy (SEM) images of CaFe-LDH; (**d**–**g**) X-ray photoelectron spectrometry (XPS) spectra (**d**,**e**,**f** and **g** show the full, O 1s,Ca 2p,Fe 2p spectra, respectively).

Fourier-transform infrared (FT-IR) analysis of CaFe-LDH was conducted to examine its functional groups, as depicted in Figure 1b. Clear LDH characteristic absorption bands were observed, with broad bands in the range of 3400 to 3700 cm^{-1} being attributed to lattice water and OH group-stretching vibrations associated with Ca^{2+} in all LDHs [18,34–36]. The absorption band at 3631 is attributed to the OH-stretching vibration from the structure of the LDH. In contrast, the absorption band at 3405 originates from water in the LDH, but primarily from hygroscopic KBr.

The band around ~1620 cm^{-1} corresponds to the bending vibration of interlayer water molecules, while the band at ~1345 cm^{-1} signifies the symmetric O-N-O stretching vibration of M-NO^{3-}. Additionally, the translational mode of the surface Fe-OH group is evident as a signal at ~1053 cm^{-1} [31].

To comprehend the valence and surface composition of CaFe-LDH, X-ray photoelectron spectroscopy (XPS) analysis was performed, as shown in Figure 1d. Peaks located at 712.08, 532.08, 386.08, 348.08, and 285.08 eV corresponded to Fe 2p, O 1s, N 1s, Ca 2p, and C 1s, respectively, providing evidence for the formation of CaFe-LDH [37]. Figure 1e demonstrated the spectral resolution of O 1s in CaFe-LDH and its deconvolution into three components. The peaks at 532.88, 531.48, and 529.88 eV were attributed to Ca-O, O-H, and Fe-O bonds, respectively, with their respective shared being 9.94%, 50.84%, and 39.22%.

The spectrum of Ca 2p shown in Figure 1f revealed peaks divided into Ca $2p_{1/2}$ (350.58 eV) and Ca $2p_{3/2}$ (347.08 eV). Similarly, the spectrum of Fe 2p in Figure 1g exhibited double peaks (Fe $2p_{1/2}$ and Fe $2p_{3/2}$) of CaFe-LDH at 724.48 and 710.88 eV, respectively, corresponding to the oxidation state of Fe^{3+} [37].

The scanning electron microscope (SEM) image of CaFe-LDH (Figure 1c) displayed the hexagonal layered structure characteristic of hydrotalcite. However, the surface appeared rougher, consisting of a stack of small fragments with attached small particles [38].

3.2. Immobilization of Cd(II) in Soil

3.2.1. Effect of Different Dosage on the Immobilization of Cd in Soil

Figure 2 shows the gradual increase in the curing efficiency of CaFe-LDH on cadmium in soil with increasing dosages. Within the dosage range of 0.001 g to 0.01 g, the curing efficiency of the active state of Cd(II) steadily rose from 60.81% to 99.63% after 24 h of reaction. This phenomenon arose from the increased content of CaFe-LDH, leading to a corresponding expansion in contact area and enhanced efficiency in immobilizing exchangeable interlayer cations [26]. Notably, at a dosage of 0.003 g, a substantial portion of the exchangeable state Cd(II) in the soil had already been completely solidified, resulting in a minimal further increase in fixation efficiency despite escalating dosages. As reported in the study by Liu et al. [39], Ca(II) in calcium-containing adsorbents can be displaced from lattice sites in water via dissolution–recrystallization processes, demonstrating an effective removal performance for heavy metals. CaFe-LDH acted as a heavy metal adsorbent, with simultaneous Ca^{2+} leaching and adsorption occurring, resulting in excellent curing properties in regard to CaFe-LDH for Cd^{2+} heavy metals. Cd(II) substitution for Ca(II) in the lattice position of the material led to isomorphic substitution.

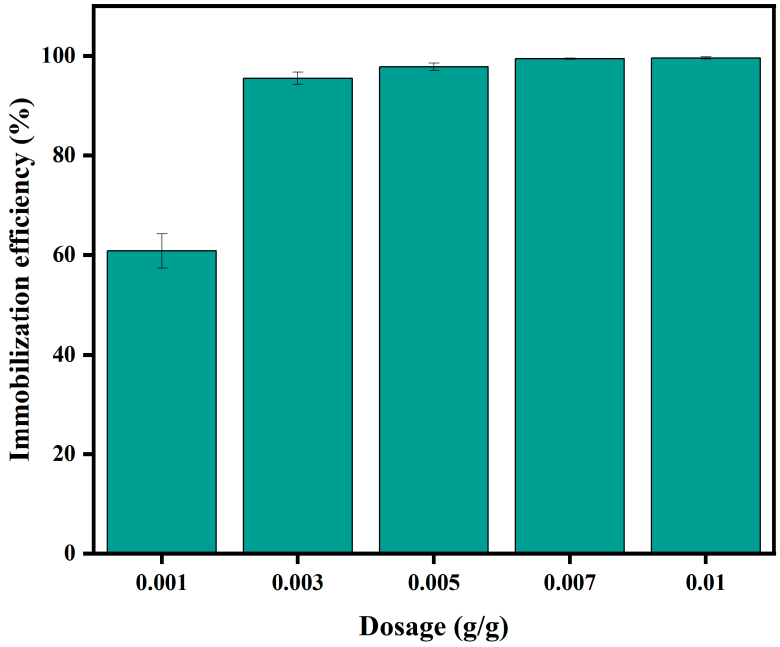

Figure 2. Immobilization of Cd(II) by different dosage of CaFe-LDH (Cd(II). Initial concentration: 2.0 mg/g, initial pH: 6.51, reaction time: 24 h).

Furthermore, when the concentration of Cd(II) remained constant, the mass transfer kinetics gradually weakened with increasing time [40]. Consequently, the rate of immobilization exhibited a negligible variation until adsorption equilibrium was attained.

3.2.2. Effect of Initial Concentration on the Immobilization of Cd in Soil

The impact of CaFe-LDH on the immobilization of Cd(II)-containing soils with varying initial concentrations is depicted in Figure 3. Maintaining a consistent dosage of 0.003 g, as the concentration of Cd(II) in the soil escalated from 500 mg/kg to 2000 mg/kg, the immobilization efficiency of CaFe-LDH on active state Cd(II) declined from 96.17% to 94.77% after 24 h of reaction, demonstrating a decreasing trend with rising concentration. This decline can be attributed to the saturation of the adsorption sites of LDH for metal ions subsequent to ion exchange, rendering it challenging for LDH to accommodate excessively high Cd(II) contents [41]. Consequently, the increase in Cd(II) concentration failed to enhance the passivation capacity of CaFe-LDH within the soil [42].

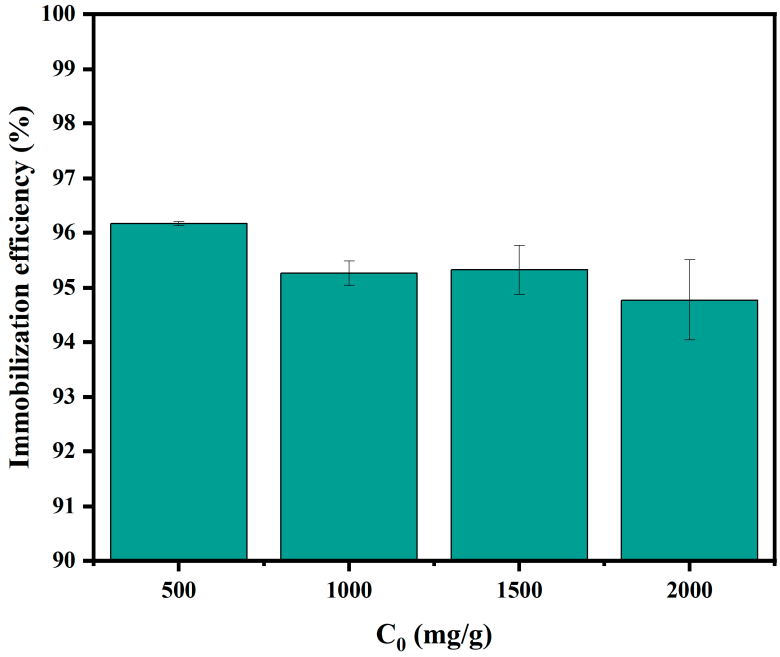

Figure 3. Effect of initial Cd(II) concentration in soil by CaFe-LDH (Initial pH: 6.51, reaction time: 24 h, amount of CaFe-LDH: 0.003 g).

3.2.3. Effect of Cd(II)-containing Contaminated Soil with Different pH on the Immobilization Effect of Cd(II)

Figure 4 illustrates the curing efficiency of 0.003 g of CaFe-LDH on 2000 mg/kg of Cd(II)-containing soil at various pH levels. In an alkaline environment, Cd(II) tends to exist as $Cd(OH)_2$ in the soil, hence the pH of the experimental soil was adjusted within the range of 4 to 6.5 [43]. Soil pH was modulated using sodium hydroxide and nitric acid, resulting in a curing efficiency of only 31.80% at pH 4, which substantially increased to 94.77% as the pH was gradually elevated. Notably, the curing capacity of CaFe-LDH on Cd(II) at low pH levels was markedly inferior to its adsorption ability at higher pH levels [44].

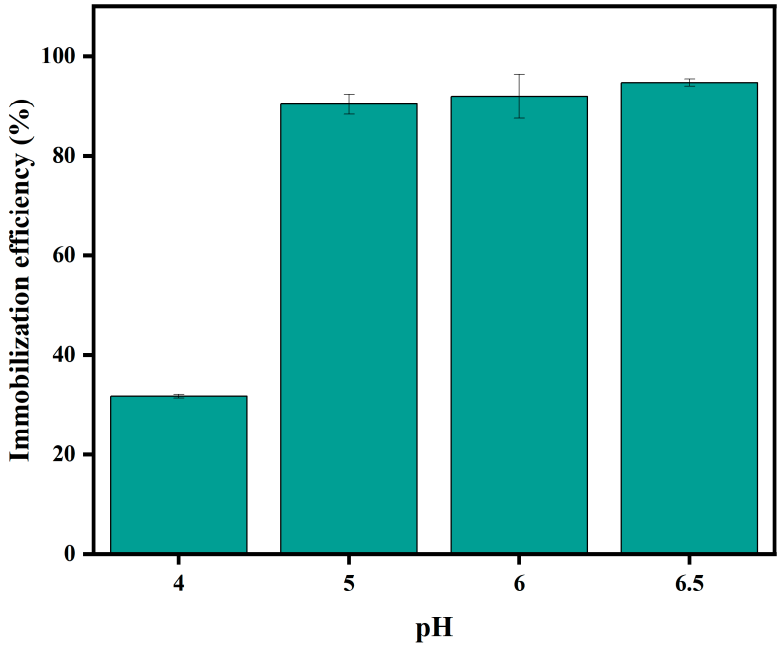

Figure 4. Effect of the initial soil pH on the immobilization of Cd(II) (Cd(II) initial concentration: 2.0 mg/g, amount of CaFe-LDH: 0.003 g, reaction time: 24 h).

The adsorption of Cd(II) by CaFe-LDH was found to increase with rising pH, a phenomenon likely attributed to the surface properties of CaFe-LDH, including surface charge and functional group dissociation [45]. The surface of CaFe-LDH was rich in binding sites, with protonation reactions occurring on the surface at a low pH, resulting in a positively charged surface. Conversely, at higher pH levels, deprotonation processes prevailed, rendering the surface of the CaFe-LDH negatively charged. As the pH increased, the positive charge density at the adsorption edge diminished, leading to reduced electrostatic repulsion and thereby enhancing the adsorption of positively charged Cd(II) ions through electrostatic attraction [18,46].

3.2.4. Morphological Analysis of Soil–Heavy Metals

Figure 5 shows the distribution of Cd forms in soil using the Tessier sequential extraction method, which enabled the analysis of morphological transformation of Cd in soil [47]. The biomorphic toxicity of Cd in soil was not only associated with TCLP leaching but also directly linked to their distribution pattern, which held significant importance for the environmental impact of Cd in soil. The results of the sequential extraction, as depicted in Figure 5, revealed that in the extraction of a 1.0 g sample of soil containing 2000 mg/L Cd(II), the total Cd content in the soil closely approximated the theoretical value. Specifically, the Cd existed in various forms, including water-soluble, exchangeable, carbonate-bound, Fe-Mn oxide-bound, organic-matter-bound, and residual states, constituting 18%, 13%, 0%, 59%, 9%, 1%, and 0% of the Cd content, respectively. Some forms with low content may not be well represented in the graph. With the application of the curing agent CaFe-LDH, the percentage of water-soluble Cd decreased from 18% to 0%, while exchangeable Cd decreased from 13% to 6%, and carbonate-bound Cd increased from 59% to 81%. Additionally, the percentages of Fe-Mn oxide-bound Cd and organic matter-bound Cd increased slightly, possibly due to the presence of a significant amount of Fe-Mn oxides in the soil itself, which tend to generate Fe-Mn oxide-bound Cd during the passivation process. Conversely, the percentage of residual Cd remained comparatively small and low. These data indicate that the Cd(II) form predominantly shifts from water-soluble and exchangeable states to the carbonate-bound state during CaFe-LDH passivation. This transformation may be attributed to the soil's inherent carbonate content and alkaline nature, which facilitate the formation of cadmium carbonate during the passivation process. Cadmium carbonate was known to be more stable and less prone to migration [42].

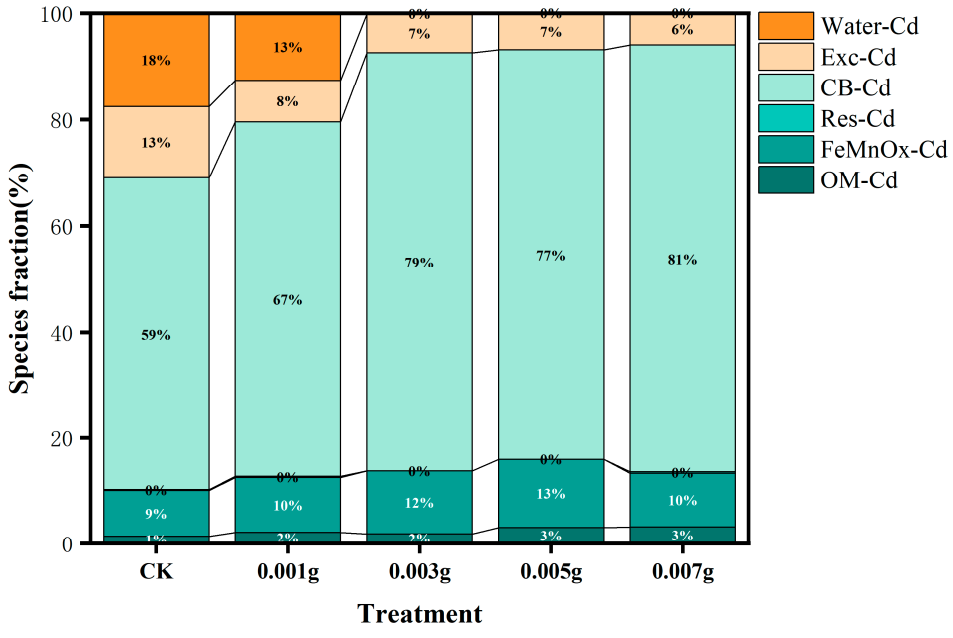

Figure 5. Percentage of different forms of Cd in soil before and after treatment (Cd(II) initial concentration: 2.0 mg/g; reaction time: 24 h).

3.3. TCLP

Figure 6 displays the TCLP leachability of soil samples before and after different treatment durations. The TCLP toxic leaching procedure served as a valuable tool for evaluating the potential environmental risks associated with Cd(II) contaminated soils by extracting the biologically active fraction of heavy metals from the soil [48]. The variation in TCLP-extractable Cd(II) content of untreated soil after various reaction times is depicted in Figure 6. It was evident from the figure that the initial Cd leaching concentration of the contaminated soil stood at 142.30 mg/L. However, after treatment with CaFe-LDH for 2 h, the Cd(II) leaching rate dropped significantly to only 48.13 mg/L. Subsequently, over the following 48 h of reaction, the leaching rate of Cd(II) remained relatively stable in the range of 30–40 mg/L without significant fluctuations. This phenomenon may be attributed to the abundance of hydroxyl groups on the surface of LDH, which, combined with the higher pH, facilitated Cd adsorption onto the surface through electrostatic forces, thereby reducing the migration rate of Cd. These findings suggested a significant decrease in the concentration of TCLP-Cd in the polluted soil following remediation with CaFe-LDH, with minimal alteration even with prolonged reaction times. CaFe-LDH demonstrated a pronounced remediation effect on soil by effectively immobilizing Cd within it. Consequently, the Cd activity in the remediated soil remained low, underscoring the efficacy of CaFe-LDH in preventing Cd migration within the soil.

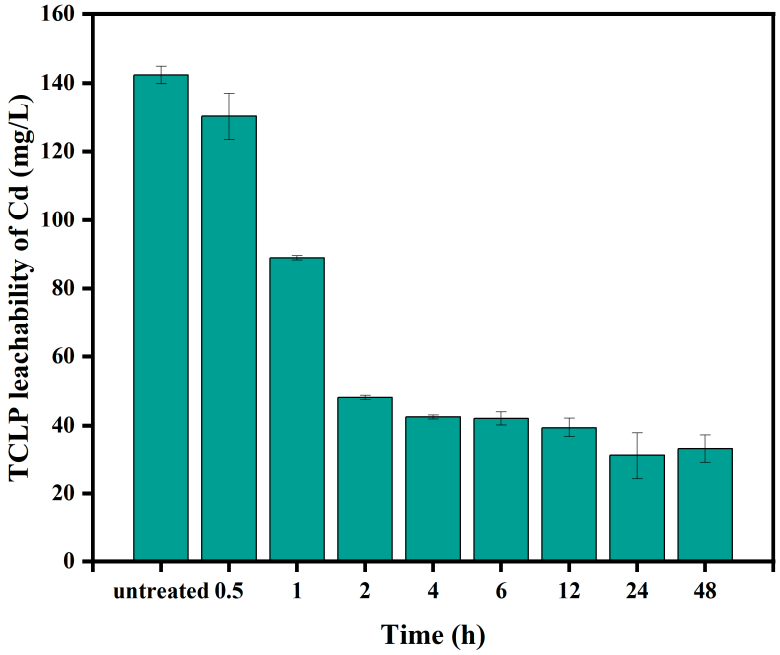

Figure 6. TCLP leachability of Cd(II) after the soil samples were treated (amount of CaFe-LDH: 0.003 g, initial pH: 6.51, room temperature(RT): 25 °C).

3.4. Soil Phytotoxicity Tests

To further investigate the toxicity of the remediated soil, mung bean seeds were selected as experimental subjects for planting culture. Toxicological indicators, such as germination rate, plant growth length, and biomass of the seeds, were recorded during the cultivation process [49].

Figure 7a illustrates that the germination rate of mung bean seeds in clean, polluted, and remediated soil was 93.3%, 80%, and 100%, respectively. Notably, the germination rate in both clean and remediated soil surpassed that of polluted soil. In clean soil conditions (Figure 7b), mung bean seeds thrived, displaying robust growth with root, stem, and leaf lengths of 32.69 mm, 211.67 mm, and 19.21 mm, respectively. Conversely, growth conditions in polluted soil were inferior, with root, stem, and leaf lengths of 26.40 mm, 17.61 mm, and 9.75 mm, respectively. The diminished growth in polluted soil can be attributed to

the adverse effects of high Cd concentration, which hindered mung bean development. However, in soil remediated with CaFe-LDH, mung bean growth flourished, exhibiting root, stem, and leaf lengths of 39.65 mm, 159.78 mm, and 18.75 mm, respectively. The significant improvement in mung bean growth in remediated soil brought the lengths of roots, stems, and leaves closer to those observed in clean soil conditions.

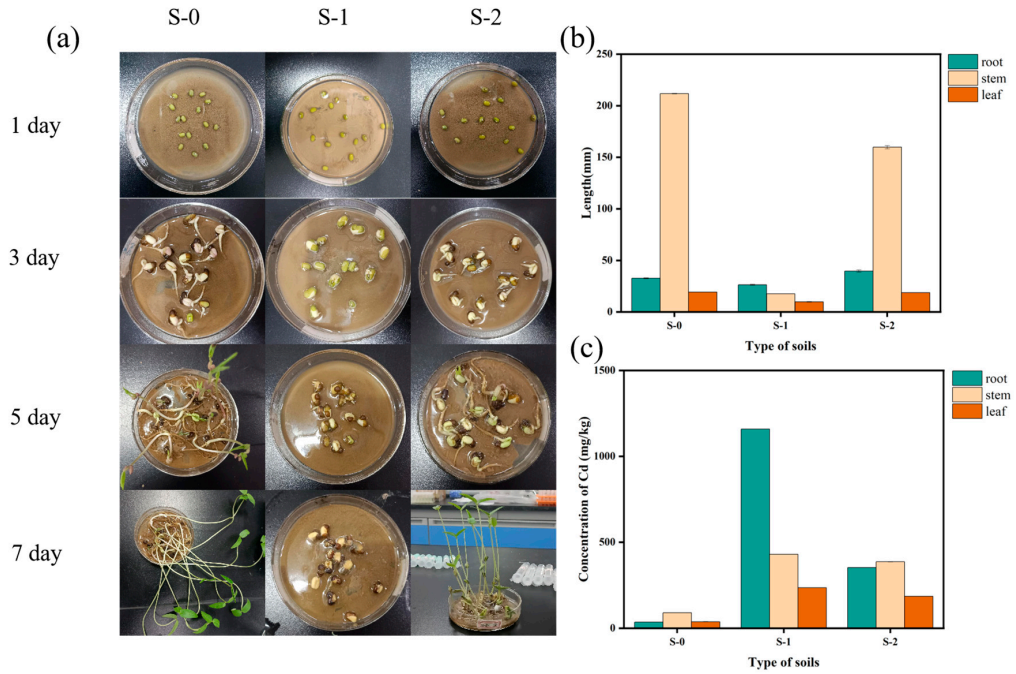

Figure 7. (**a**) Photographs of the plant cultivation process; (**b**) length and (**c**) Cd concentration of roots, and leaves of in different soil samples for ten days. (S-0, S-1, S-2 represent clean soil, Cd(II)-contaminated soil, and CaFe-LDH treated soil).

The accumulation of Cd in mung bean plants is depicted in Figure 7c, where the Cd content in roots, stems, and leaves in the remediated soil (S-2) significantly decreased compared to the polluted soil (S-1), with values of 352.5 mg/kg, 386.3 mg/kg, and 185.6 mg/kg, respectively. This reduction indicated that CaFe-LDH effectively inhibited the migration of Cd, demonstrating its superior soil remediation performance [50].

3.5. Analysis of the Immobilization Mechanism

Figure 8a presents the morphology of hydrotalcite after the reaction with Cd. Despite the reaction, CaFe-LDH maintained its hexagonal layer structure akin to hydrotalcite. However, irregular lumps of solids were observed alongside the stacked fragments, likely resulting from other substances in the soil adhering to the hydrotalcite surface post-reaction [51].

The XRD pattern of the reacted CaFe-LDH is depicted in Figure 8b. It still exhibited characteristic diffraction peaks of hydrotalcite. Past studies had indicated that the solubility of Cd hydroxide was lower than that of calcium hydroxide, leading to partial dissolution of hydrotalcite during the Cd curing process. The absence of characteristic peaks of $Cd(OH)_2$ and $CdCO_3$ in the XRD pattern suggested the absence of surface precipitation of CaFe-LDH during Cd^{2+} adsorption [44]. Moreover, the positively charged layer of LDH hindered Cd^{2+} adsorption by electrostatic attraction. The ionic radius of Ca^{2+} (1.00 Å) closely resembled that of Cd^{2+} (0.99 Å), and the solubility product constant of $Ca(OH)_2$ ($Ksp = 4.8 \times 10^{-5}$) was significantly lower than that of $Cd(OH)_2$ ($Ksp = 7.2 \times 10^{-15}$) [52]. This aligned with reported results indicating a positive correlation between the Ksp of LDH and the Ksp of corresponding hydroxides, suggesting the thermodynamic favorability of a Cd homocrystal substitution for Ca in CaFe-LDH layers [53]. Cd was immobilized through isomorphic substitution and solvation-reconstruction, resulting in the formation of a super-stable

mineralized structure, Cd-Fe-LDH, with reduced solubility of metal ions, which allows for long-term remediation [54].

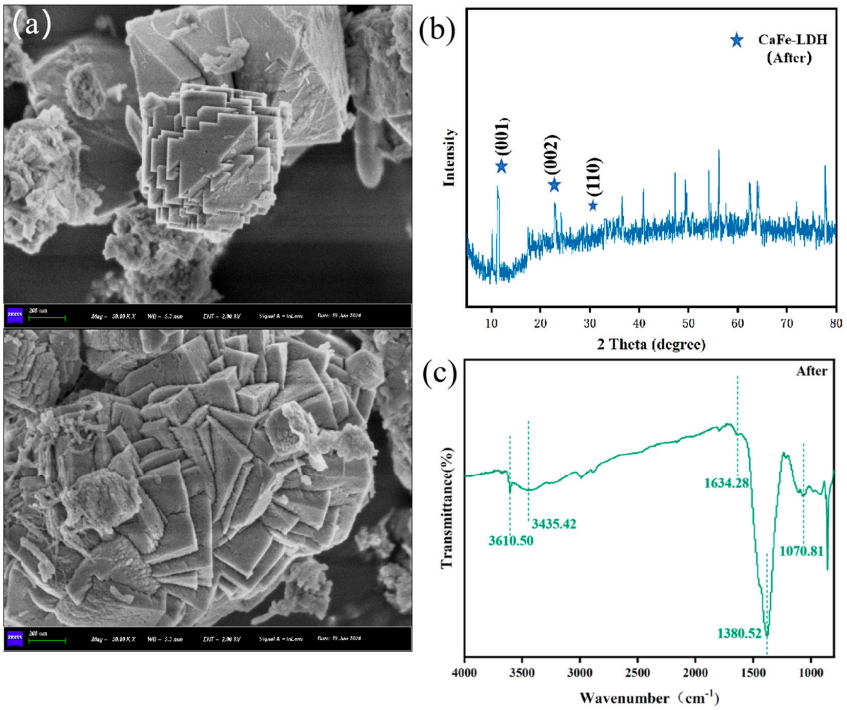

Figure 8. (**a**) Scanning electron microscopy (SEM) images of CaFe-LDH(after); (**b**) XRD pattern of CaFe-LDH(after); (**c**) Fourier-transform infrared spectra of CaFe-LDH(after).

The FTIR spectrum, as shown in Figure 8c, gave the changes in the functional groups after the reaction. After the reaction of CaFe-LDH with Cd, the stretching (3435 cm^{-1}) and bending (1634 cm^{-1}) vibrations of the hydroxyl group did not change significantly, and stretching and bending vibrations still occurred [55]. The appearance of CO_3^{2-} replacing the original NO_3^- indicated a complete exchange of NO_3^- between the layers. The characteristic bands were attributed to the overlap of various types of CO_3^{2-} , such as soil soluble salts ($CaCO_3$) and dissolved CO_2 in deionized water [56]. The mechanism of Cd immobilization in soil by CaFe-LDH is depicted in Figure 9. It involves three main steps: first, complexation is dependent on electrostatic attraction provided by protonated hydroxyl groups on the surface; second, a metal hydroxide and interlayer anion exchange occurs; and third, isomorphic substitutions between Cd and lattice elements occur.

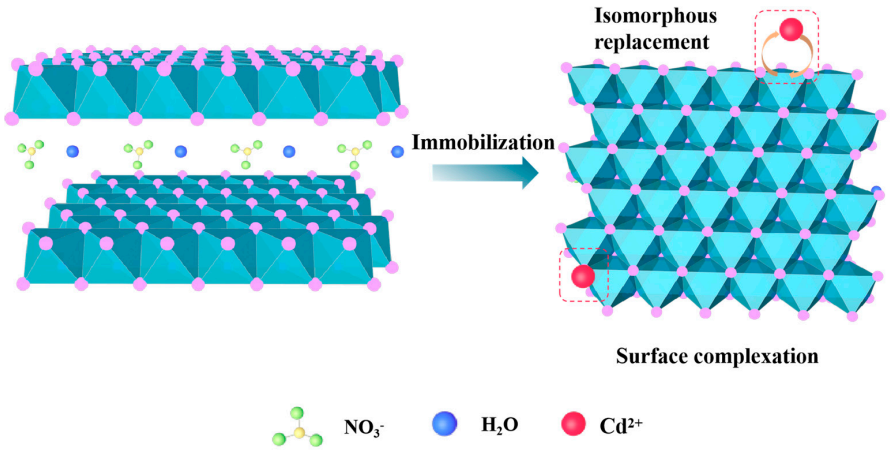

Figure 9. Immobilization mechanism of Cd onto CaFe-LDH.

As seen in Figure 9, this study has successfully prepared a simple yet highly efficient CaFe-LDH material. When a designated quantity of CaFe-LDH is dispersed in soil, CaO6 is released from the CaFe-LDH laminate into the water, owing to the superior solubility of $Ca(OH)_2$ compared to $Fe(OH)_3$. This process leads to the formation of a large surface area amorphous FeOOH structure with porous characteristics. The CaFe-LDH exhibits exceptional properties as an adsorbent for heavy metals. Concurrently, leaching and adsorption of Ca^{2+} occur, resulting in outstanding immobilization performance for Cd^{2+} heavy metals. The immobilization mechanisms encompass isomorphic substitution, surface complexation, and induced precipitation, all contributing to the material's remarkable effectiveness.

Regarding its research prospects, the calcium–iron-layered double hydroxide (CaFe-LDH) immobilization agent we have developed possesses numerous active sites and absorption pathways for Cd, enabling it to adsorb coexisting heavy metals simultaneously. Its strong affinity for heavy metals translates into high immobilization efficiency during the stabilization process. Moreover, its exceptional stability, along with its straightforward synthesis, low cost, and environmental friendliness, holds promise for practical applications. Notably, its inherent magnetism allows for the utilization of an electromagnetic separator in the recycling process, facilitating its recovery and treatment for secondary utilization, thereby minimizing secondary environmental pollution and reducing costs.

Figure 10e depicts the XPS analysis of the reacted material, revealing characteristic peaks of Cd 3d, with band energies of 405.48 eV ($3d_{5/2}$) and 412 eV ($3d_{3/2}$), respectively. These peaks confirm the presence of the Cd species on the immobilization agent post-reaction with Cd, indicating the incorporation of Cd into the interlayer structure [37]. In Figure 10b, the spectra of the O1s were presented, showcasing the distribution of the Ca-O, O-H, and Fe-O bonds. The percentages of these bonds were determined to be 22.62%, 56.98%, and 20.40%, respectively [57]. Interestingly, the percentage of Fe-O bonding decreased, while Ca-O and O-H bonds showed an increase in percentage. This shift in bond percentages suggested alterations in the chemical environment post-reaction, possibly indicating changes in the surface chemistry and interaction with Cd [44].

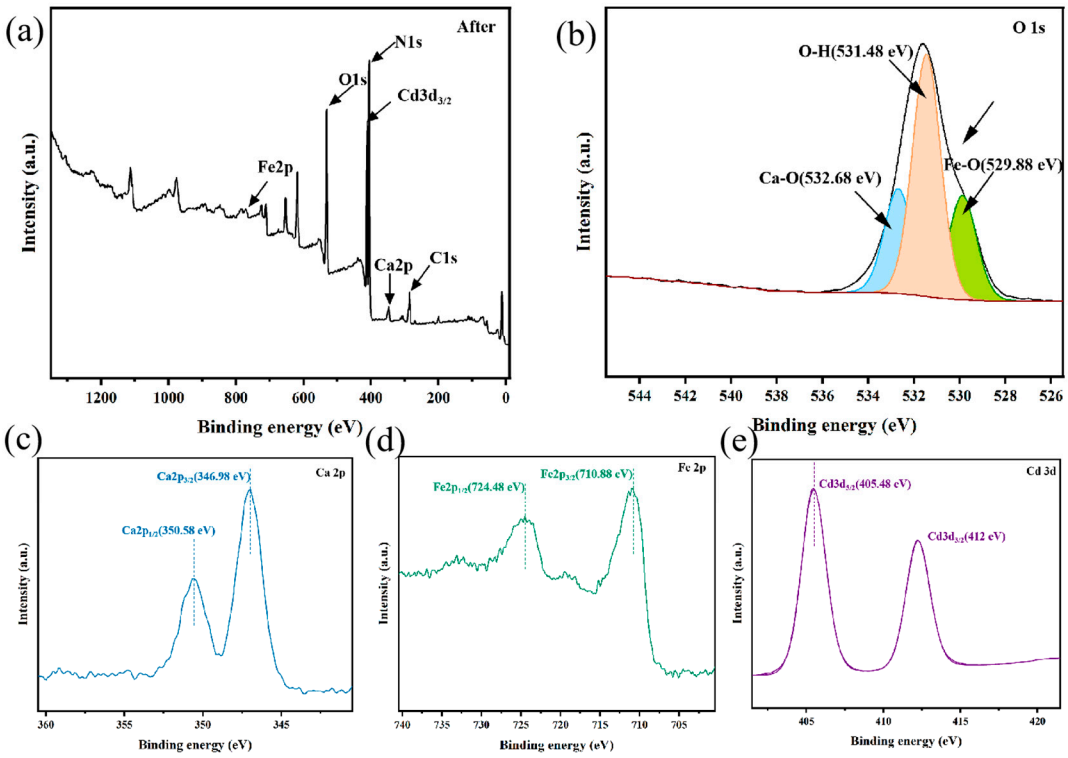

Figure 10. X-ray photoelectron spectrometry (XPS) spectra of CaFe-LDH(after) (**a**,**b**,**c**,**d** and **e** show the full, O 1s,Ca 2p,Fe 2p,Cd 3d spectra, respectively).

Figure 11 illustrates the EDS energy spectrum obtained after the reaction with Cd, revealing the elemental composition of CaFe-LDH (after). The spectrum indicated predominant presence of elements such as C, N, O, Ca, Fe, and Cd, uniformly distributed throughout the nanosheet framework [58]. This confirmed the incorporation of Cd into the CaFe-LDH structure. Additionally, the presence of elemental Cd was further confirmed by XPS measurements.

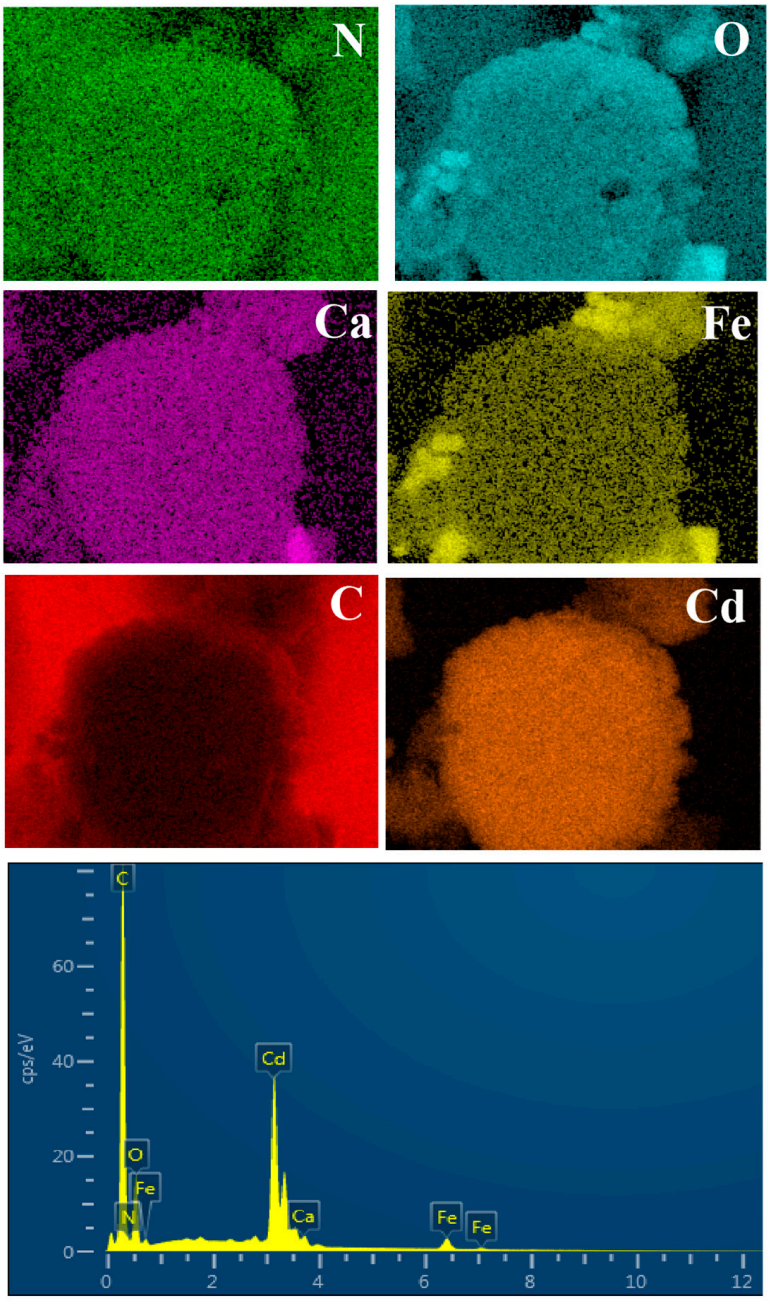

Figure 11. EDS image of CaFe-LDH after reaction.

3.6. Recovery of CaFe-LDH

The relationship between magnetization intensity and magnetic field is depicted in Figure 12c. Magnetizing CaFe-LDH resulted in a narrow hysteresis loop, weak coercivity (-Hc), and remanent magnetization (Mr), indicating its soft magnetic nature, which is capable of generating high permeability under transient magnetic fields. The magnetic permeability of CaFe-LDH reached a small maximum value at a magnetic field strength

of 17.34 Gs [59]. Subsequently, as the magnetic field strength increased, the material's magnetization strength peaked at 5.86 emu/g under an external magnetic field strength of 19,120.7 Gs. The presence of a very weak hysteresis and saturation magnetization suggested excellent superparamagnetism in CaFe-LDH, enabling rapid separation from solid matrices under an external magnetic field [60].

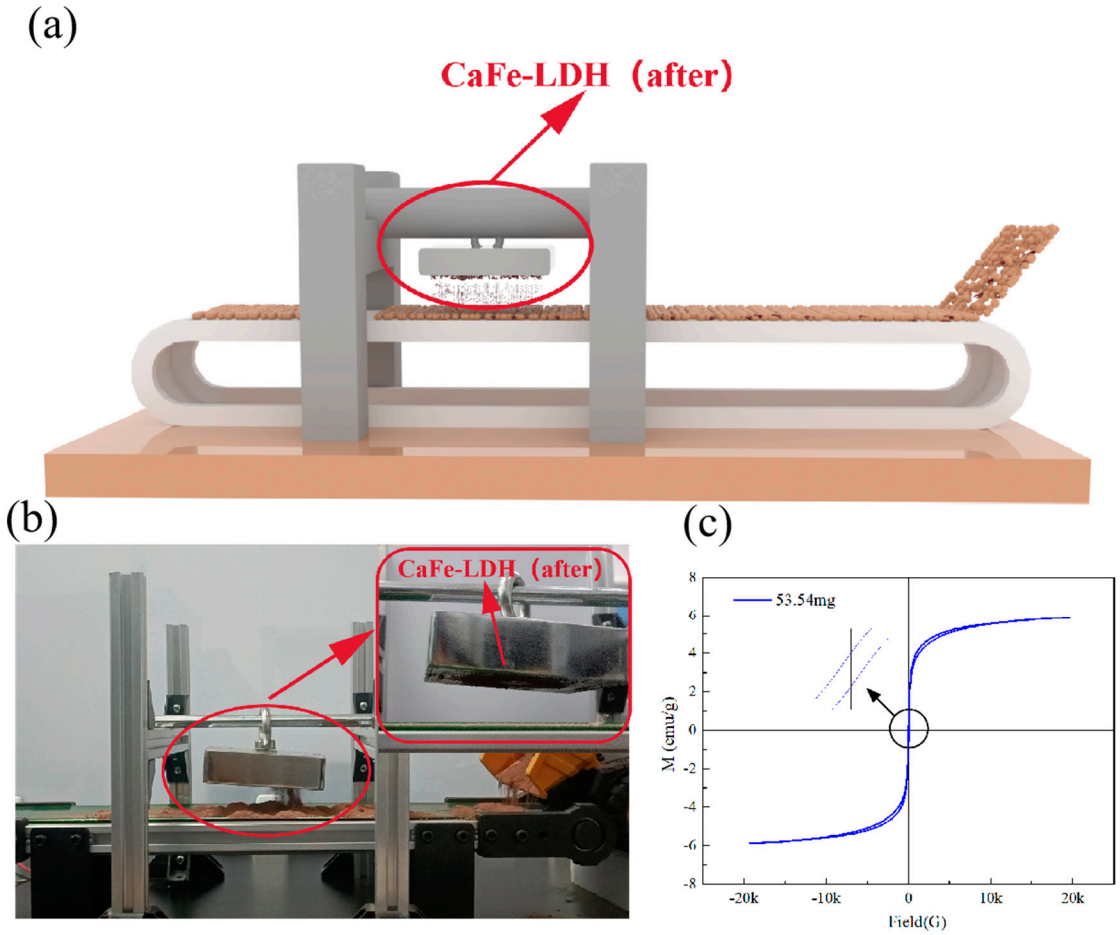

Figure 12. (**a**) Model diagram of magnetic recovery system of CaFe-LDH; (**b**) practical application diagram of magnetic recovery system; (**c**) the magnetization of CaFe-LDH.

The magnetic recovery system consists of three components: the added substance, magnetic separation, and recovery, as illustrated in Figure 12a,b. The added substance referred to the soil solidified by CaFe-LDH. While the VSM analysis indicated maximum magnetization strength at a magnetic field strength of 19120.7 Gs, experiments revealed that a permanent magnet of 3000–5000 Gs, placed 10–20 cm away from the material, could effectively induce separation. The remediated mixture was collected, and the soil was dried and stored [61]. Subsequently, the dried soil was conveyed and dumped into a material cart at a rate of 20–30 cm^3/min, with the conveyor speed matching the material dumping rate. As the LDHs-M beads traversed the magnetic field area, they were attracted to the magnet, whereas soil without beads was transported to a recovery tank at the conveyor belt's tail end (video) [28].

4. Conclusions

In conclusion, this study effectively synthesized CaFe-LDH and employed it to remediate Cd(II)-contaminated soil. LDH played a crucial role in the immobilization process, exhibiting significant immobilization properties with a maximum Cd(II) adsorption capacity of 31.10 mg/L. The TCLP experiment results demonstrated the efficient immobilization of Cd(II) by CaFe-LDH, with removal efficiency increasing from 31.8% to 94.77%, being

particularly sensitive to the initial soil pH between 4 and 6.5. Mechanistic assessments using FT-IR, SEM, XRD, and XPS revealed that isomorphous substitution and surface adsorption were primary mechanisms for immobilizing Cd(II). Additionally, the presence of surface hydroxyl functional groups on hydrotalcite provides Cd(II) complex adsorption sites. The recycling application of CaFe-LDH offered a promising approach to addressing the challenge of heavy metal cleanup and passivation.

Author Contributions: Conceptualization, X.Q.; methodology, Y.J.; software, Y.J.; validation, R.C., J.Z. and L.H.; formal analysis, Y.J.; investigation, Y.J., R.C., J.Z. and L.H.; resources, X.Q.; data curation, R.C., J.Z. and L.H.; writing—original draft preparation, Y.J.; writing—review and editing, X.Q. and Y.J.; visualization, Y.J.; supervision, X.Q.; project administration, X.Q.; funding acquisition, X.Q. All authors have read and agreed to the published version of the manuscript.

Funding: This research was funded by National Natural Science Foundation of China, grant number 41703119 and 51504170, Innovative Team program of Natural Science Foundation of Hubei Province, grant number 2021CFA032, and Open founding of Wuhan institute of technology Jingmen research institute of new chemical materials industry technology (JM2023001).

Data Availability Statement: Data are available on request from the authors. The data are not publicly available due to Laboratory data.

Acknowledgments: Shiyanjia Lab (www.shiyanjia.com) for the XPS analysis.

Conflicts of Interest: The authors declare no conflict of interest.

References

1. Valverde, M.; Fortoul, T.I.; Díaz-Barriga, F.; Mejia, J.; Del Castillo, E.R. Induction of genotoxicity by cadmium chloride inhalation in several organs of CD-1 mice. *Mutagenesis* **2000**, *15*, 109–114. [CrossRef]
2. Zhao, H.; Du, L.; Wu, Y.; Wu, X.; Han, W. Numerical assessment of the passivator effectiveness for Cd-contaminated soil remediation. *Sci. Total. Environ.* **2021**, *779*, 146485. [CrossRef]
3. Grygar, T.M.; Faměra, M.; Hošek, M.; Elznicová, J.; Rohovec, J.; Matoušková, S.; Navrátil, T. Uptake of Cd, Pb, U, and Zn by plants in floodplain pollution hotspots contributes to secondary contamination. *Environ. Sci. Pollut. Res.* **2021**, *28*, 51183–51198. [CrossRef]
4. Du Laing, G.; Rinklebe, J.; Vandecasteele, B.; Meers, E.; Tack, F.M.G. Trace metal behaviour in estuarine and riverine floodplain soils and sediments: A review. *Sci. Total. Environ.* **2009**, *407*, 3972–3985. [CrossRef]
5. Shaheen, S.M.; Rinklebe, J. Impact of emerging and low cost alternative amendments on the (im)mobilization and phytoavailability of Cd and Pb in a contaminated floodplain soil. *Ecol. Eng.* **2015**, *74*, 319–326. [CrossRef]
6. Liu, L.; Li, W.; Song, W.; Guo, M. Remediation techniques for heavy metal-contaminated soils: Principles and applicability. *Sci. Total Environ.* **2018**, *633*, 206–219. [CrossRef]
7. He, Z.; Shentu, J.; Yang, X.; Baligar, V.C.; Zhang, T.; Stoffella, P.J. Heavy metal contamination of soils: Sources, indicators and assessment. *J. Environ. Indic.* **2015**, *9*, 17–18.
8. Huang, Y.; Wang, L.; Wang, W.; Li, T.; He, Z.; Yang, X. Current status of agricultural soil pollution by heavy metals in China: A meta-analysis. *Sci. Total. Environ.* **2019**, *651*, 3034–3042. [CrossRef]
9. Liu, X.; Tian, G.; Jiang, D.; Zhang, C.; Kong, L. Cadmium (Cd) distribution and contamination in Chinese paddy soils on national scale. *Environ. Sci. Pollut. Res.* **2016**, *23*, 17941–17952. [CrossRef] [PubMed]
10. Khalid, S.; Shahid, M.; Niazi, N.K.; Murtaza, B.; Bibi, I.; Dumat, C. A comparison of technologies for remediation of heavy metal contaminated soils. *J. Geochem. Explor.* **2017**, *182*, 247–268. [CrossRef]
11. Li, Z.; Zhang, J.; Qu, C.; Tang, Y.; Slaný, M. Synthesis of Mg-Al Hydrotalcite Clay with High Adsorption Capacity. *Materials* **2021**, *14*, 7231. [CrossRef]
12. Cui, J.; Wang, W.; Peng, Y.; Zhou, F.; He, D.; Wang, J.; Chang, Y.; Yang, J.; Zhou, J.; Wang, W.; et al. Effects of simulated Cd deposition on soil Cd availability, microbial response, and crop Cd uptake in the passivation-remediation process of Cd-contaminated purple soil. *Sci. Total. Environ.* **2019**, *683*, 782–792. [CrossRef]
13. Hamid, Y.; Tang, L.; Yaseen, M.; Hussain, B.; Zehra, A.; Aziz, M.Z.; He, Z.-L.; Yang, X. Comparative efficacy of organic and inorganic amendments for cadmium and lead immobilization in contaminated soil under rice-wheat cropping system. *Chemosphere* **2019**, *214*, 259–268. [CrossRef] [PubMed]
14. Gu, X.; Evans, L.J.; Barabash, S.J. Modeling the adsorption of Cd (II), Cu (II), Ni (II), Pb (II) and Zn (II) onto montmorillonite. *Geochim. Cosmochim. Acta Suppl.* **2010**, *74*, 5718–5728. [CrossRef]
15. Jiang, M.; Jin, X.; Lu, X.; Chen, Z. Adsorption of Pb(II), Cd(II), Ni(II) and Cu(II) onto natural kaolinite clay. *Desalination* **2010**, *252*, 33–39. [CrossRef]

16. Kong, X.; Ge, R.; Liu, T.; Xu, S.; Hao, P.; Zhao, X.; Li, Z.; Lei, X.; Duan, H. Super-stable mineralization of cadmium by calcium-aluminum layered double hydroxide and its large-scale application in agriculture soil remediation. *Chem. Eng. J.* **2021**, *407*, 127178. [CrossRef]
17. Behbahani, E.S.; Dashtian, K.; Ghaedi, M. Fe_3O_4-$FeMoS_4$: Promise magnetite LDH-based adsorbent for simultaneous removal of Pb (II), Cd (II), and Cu (II) heavy metal ions. *J. Hazard.* **2021**, *410*, 124560. [CrossRef]
18. Shan, R.; Yan, L.; Yang, K.; Hao, Y.; Du, B. Adsorption of Cd(II) by Mg-Al-CO_3- and magnetic Fe_3O_4/Mg-Al-CO_3-layered double hydroxides: Kinetic, isothermal, thermodynamic and mechanistic studies. *J. Hazard.* **2015**, *299*, 42–49. [CrossRef] [PubMed]
19. Argane, R.; Adnani, M.E.; Benzaazoua, M.; Bouzahzah, H.; Khalil, A.; Hakkou, R.; Taha, Y. Geochemical behavior and environmental risks related to the use of abandoned base-metal tailings as construction material in the upper-Moulouya district, Morocco. *Environ. Sci. Pollut. Res.* **2016**, *23*, 612. [CrossRef]
20. Azimzadeh, Y.; Najafi, N.; Reyhanitabar, A.; Oustan, S.; Khataee, A. Effects of phosphate loaded LDH-biochar /hydrochar on maize dry matter and P uptake in a calcareous soil. *Arch. Agron. Soil. Sci.* **2021**, *67*, 1649–1664. [CrossRef]
21. Feng, Y.; Yang, J.; Liu, W.; Yan, Y.; Wang, Y. Hydroxyapatite as a passivator for safe wheat production and its impacts on soil microbial communities in a Cd-contaminated alkaline soil. *J. Hazard. Mater.* **2021**, *404*, 124005. [CrossRef] [PubMed]
22. Wang, W.; Shu, Y.; Xiang, H.; Xu, D.; Zhang, P.; Ren, G.; Zhong, Y.; Yang, X. Magnetic properties of $Cu_{0.5}Mg_{0.5}Fe_2O_4$ nanoparticles synthesized with waste ferrous sulfate. *Mater. Today. C* **2020**, *25*, 101516. [CrossRef]
23. Pan, J.; Gao, B.; Duan, P.; Guo, K.; Xu, X.; Yue, Q. Recycling exhausted magnetic biochar with adsorbed Cu^{2+} as a cost-effective permonosulfate activator for norfloxacin degradation: Cu contribution and mechanism. *J. Hazard. Mater.* **2021**, *413*, 125413. [CrossRef] [PubMed]
24. Li, Z.; Zhang, X.; Chen, J.; Fang, X.; Yuan, W.; Yu, J.; Qiu, X. Preparing of layered double hydroxide- alginate microspheres for Cr(VI)-contaminated soil remediation. *Colloids Surf. A* **2023**, *658*, 130655. [CrossRef]
25. Xiang, Y.; Xiang, Y.; Jiao, Y.; Wang, L. Surfactant-modified magnetic CaFe-layered double hydroxide for improving enzymatic saccharification and ethanol production of Artemisia ordosica. *Renew. Energ.* **2019**, *138*, 465–473. [CrossRef]
26. Dinari, M.; Roghani, N. Calcium Iron Layered Double Hydroxide/Poly(vinyl chloride) Nanocomposites: Synthesis, Characterization and Cd^{2+} Removal Behavior. *J. Inorg. Organomet. Polym. Mater.* **2020**, *30*, 808–819. [CrossRef]
27. Wu, Y.; Yu, Y.; Zhou, J.Z.; Liu, J.; Chi, Y.; Xu, Z.P.; Qian, G. Effective removal of pyrophosphate by Ca-Fe-LDH and its mechanism. *Chem. Eng. J.* **2012**, *179*, 72–79. [CrossRef]
28. Intachai, S.; Nakorn, M.N.; Kaewnok, A.; Pankam, P.; Sumanatrakul, P.; Khaorapapong, N. Versatile inorganic adsorbent for efficient and practical removal of hexavalent chromium in water. *Mater. Chem. Phys.* **2022**, *288*, 126388. [CrossRef]
29. Costantino, U.; Bugatti, V.; Gorrasi, G.; Montanari, F.; Nocchetti, M.; Tammaro, L.; Vittoria, V. New polymeric composites based on poly(-caprolactone) and layered double hydroxides containing antimicrobial species. *ACS Appl. Mater. Interfaces.* **2009**, *1*, 668–677. [CrossRef]
30. Kim, R.; Yoon, J.; Kim, T.; Yang, J.E.; Owens, G.; Kim, K.R. Bioavailability of heavy metals in soils: Definitions and practical implementation—A critical review. *Environ. Geochem. Health* **2015**, *37*, 1041–1061. [CrossRef]
31. Szabados, M.; Ádám, A.A.; Kónya, Z.; Kukovecz, Á.; Carlson, S.; Sipos, P.; Pálinkó, I. Effects of ultrasonic irradiation on the synthesis, crystallization, thermal and dissolution behaviour of chloride-intercalated, co-precipitated CaFe-layered double hydroxide. *Ultrason. Sonochem.* **2019**, *55*, 165–173. [CrossRef] [PubMed]
32. Chen, C.; Tao, L.; Du, S.; Chen, W.; Wang, Y.; Zou, Y.; Wang, S. Advanced Exfoliation Strategies for Layered Double Hydroxides and Applications in Energy Conversion and Storage. *Adv. Funct.* **2020**, *30*, 1909832. [CrossRef]
33. Sipiczki, M.; Kuzmann, E.; Homonnay, Z.; Megyeri, J.; Palinko, I.; Sipos, P. The structure and stability of CaFe layered double hydroxides with various Ca:Fe ratios studied by Mossbauer spectroscopy, X-ray diffractometry and microscopic analysis. *J. Mol. Struct.* **2013**, *1044*, 116–120. [CrossRef]
34. Chen, Y.; Shui, Z.; Chen, W.; Chen, G. Chloride binding of synthetic Ca-Al-NO_3 LDHs in hardened cement paste. *Constr. Build. Mater.* **2015**, *93*, 1051–1058. [CrossRef]
35. Wang, J.; Wang, X.; Tan, L.; Chen, Y.; Hayat, T.; Hu, J.; Alsaedi, A.; Ahmad, B.; Guo, W.; Wang, X. Performances and mechanisms of Mg/Al and Ca/Al layered double hydroxides for graphene oxide removal from aqueous solution. *Chem. Eng. J.* **2016**, *297*, 106–115. [CrossRef]
36. Qu, Z.Y.; Yu, Q.L.; Brouwers, H.J.H. Relationship between the particle size and dosage of LDHs and concrete resistance against chloride ingress. *Cement. Concrete. Res.* **2018**, *105*, 81–90. [CrossRef]
37. Yang, L.; Chen, M.; Lu, Z.; Huang, Y.; Wang, J.; Lu, L.; Cheng, X. Synthesis of CaFeAl layered double hydroxides 2D nanosheets and the adsorption behaviour of chloride in simulated marine concrete. *Cem. Concr. Compos.* **2020**, *114*, 103817. [CrossRef]
38. Li, Z.; Zheng, S.; Yan, J.; Qian, P.; Ye, S. Design and preparation of CaFe layered double hydroxides for efficient treatment of fluorinated water deduced by tailored sustained-release of Ca^{2+}. *Chem. Eng. J.* **2024**, *480*, 147950. [CrossRef]
39. Liu, T.; Yang, J.; Ji, K.; Zheng, M.; Yang, X.; Shao, M.; Duan, H.; Kong, X. Multiple Anchor Sites of CaFe-LDH Enhanced the Capture Capacity to Cadmium, Arsenite, and Lead Simultaneously in Contaminated Water/Soil: Scalable Synthesis, Mechanism, and Validation. *ACS ES&T Eng.* **2024**, *4*, 550–561.
40. Chi, H.; Wang, J.; Wang, H.; Li, S.; Yang, M.; Bai, S.; Li, C.; Sun, X.; Zhao, Y.; Song, Y. Super-Stable Mineralization of Ni^{2+} Ions from Wastewater using CaFe Layered Double Hydroxide. *Adv. Funct. Mater.* **2021**, *32*, 2106645. [CrossRef]

41. Wang, Y.; Tang, X.; Chen, Y.; Zhan, L.; Li, Z.; Tang, Q. Adsorption behavior and mechanism of Cd(II) on loess soil from China. *J. Mol. Struct.* **2009**, *172*, 30–37. [CrossRef] [PubMed]
42. Zhang, S.; Chen, J.; Yu, J.; Yu, Q.; Qiu, X. Remediation of Cd-contaminated soil through different layered double hydroxides: The weakness of delamination and mechanism. *J. Environ. Chem. Eng.* **2022**, *10*, 107815. [CrossRef]
43. Hong, C.O.; Owens, V.N.; Kim, Y.G.; Lee, S.M.; Park, H.C.; Kim, K.K.; Son, H.J.; Suh, J.M.; Kim, P.J. Soil pH Effect on Phosphate Induced Cadmium Precipitation in Arable Soil. *Bull. Environ. Contam. Toxicol.* **2014**, *93*, 101–105. [CrossRef] [PubMed]
44. Liang, X.; Su, Y.; Wang, X.; Liang, C.; Tang, C.; Wei, J.; Liu, K.; Ma, J.; Yu, F.; Li, Y. Insights into the heavy metal adsorption and immobilization mechanisms of CaFe-layered double hydroxide corn straw biochar: Synthesis and application in a combined heavy metal-contaminated environment. *Chemosphere* **2023**, *313*, 137467. [CrossRef] [PubMed]
45. Liu, Z.; Zhou, Q.; Hong, Z.; Xu, R. Effects of Surface Charge and Functional Groups on the Adsorption and Binding Forms of Cu and Cd on Roots of indica and japonica Rice Cultivars. *Front. Recent Dev. Plant Sci.* **2017**, *8*, 1489. [CrossRef] [PubMed]
46. Zhao, D.; Sheng, G.; Hu, J.; Chen, C.; Wang, X. The adsorption of Pb(II) on Mg_2Al layered double hydroxide. *Chem. Eng. J.* **2011**, *171*, 167–174. [CrossRef]
47. Pan, Y.; Fu, Y.; Liu, S.; Ma, T.; Tao, X.; Ma, Y.; Fan, S.; Dang, Z.; Lu, G. Spatial and temporal variations of metal fractions in paddy soil flooding with acid mine drainage. *Environ. Res.* **2022**, *212*, 113241. [CrossRef] [PubMed]
48. Zhao, J.; Zhang, L.; Zhang, S.; Yuan, W.; Fang, X.; Yu, Q.; Qiu, X. Remediation of chromium-contaminated soil using calcined layered double hydroxides containing different divalent metals: Temperatures and mechanism. *Chem. Eng. J.* **2021**, *425*, 131405. [CrossRef]
49. Wang, Y.; Fang, Z.; Kang, Y.; Tsang, E.P. Immobilization and phytotoxicity of chromium in contaminated soil remediated by CMC-stabilized nZVI. *J. Hazard. Mater.* **2014**, *275*, 230–237. [CrossRef]
50. Yu, F.; Gu, T.; Wei, J.; Tang, C.; Li, S.; Chen, Y.; Su, Y.; Liu, K.; Ma, J.; Liang, X.; et al. CaFe-layered double hydroxide corn straw biochar reduced heavy metal uptake by *Brassica campestris* L. and *Ipomoea aquatic* F.: Rhizosphere effects and oxidative stress alleviation. *JEM* **2023**, *330*, 117227. [CrossRef]
51. He, T.; Sun, J.; Deng, L.; Ming, J.; Hu, C. Recycling Fe and improving organic pollutant removal via in situ forming magnetic core-shell Fe_3O_4@CaFe-LDH in Fe (II)-catalyzed oxidative wastewater treatment. *J. Environ. Chem. Eng.* **2025**, *147*, 523–537. [CrossRef]
52. Kutus, B.; Gácsi, A.; Pallagi, A.; Pálinkó, I.; Peintler, G.; Sipos, P. A comprehensive study on the dominant formation of the dissolved $Ca(OH)_{2(aq)}$ in strongly alkaline solutions saturated by Ca(ii). *RSC Adv.* **2016**, *6*, 45231–45240. [CrossRef]
53. Qian, G.; Feng, L.; Zhou, J.Z.; Xu, Y.; Liu, J.; Zhang, J.; Xu, Z.P. Solubility product (Ksp)-controlled removal of chromate and phosphate by hydrocalumite. *Chem. Eng. J.* **2012**, *181–182*, 251–258. [CrossRef]
54. Sun, Z.; Wang, Y.; Liu, T.; Kong, X.; Pan, T.; Zhang, F.; Lei, X.; Duan, X. Super-stable mineralization of Cu, Cd, Zn and Pb by CaAl-layered double hydroxide: Performance, mechanism, and large-scale application in agriculture soil remediation. *J. Hazard. Mater.* **2023**, *447*, 130723. [CrossRef] [PubMed]
55. Grishchenko, R.O.; Emelina, A.L.; Makarov, P.Y. Thermodynamic properties and thermal behavior of Friedel's salt. *Thermochimica Acta.* **2013**, *570*, 74–79. [CrossRef]
56. Ren, H.; Qing, K.; Chen, Y.; Lin, Y.; Duan, X. Smoke suppressant in flame retarded thermoplastic polyurethane composites: Synergistic effect and mechanism study. *Nano. Res.* **2021**, *14*, 3926–3934. [CrossRef]
57. Liao, W.; Wang, H.; Li, H.Q.; Yang, P. Cd(ii) removal by Fe(ii) surface chemically modified layered double hydroxide-graphene oxide: Performance and mechanism. *Rsc. Adv.* **2019**, *9*, 38982–38989. [CrossRef] [PubMed]
58. Guan, X.; Yuan, X.; Zhao, Y.; Bai, J.; Li, Y.; Cao, Y.; Chen, Y.; Xiong, T. Adsorption behaviors and mechanisms of Fe/Mg layered double hydroxide loaded on bentonite on Cd (II) and Pb (II) removal. *J. Colloid Interface Sci.* **2022**, *612*, 572–583. [CrossRef]
59. Saiah, F.B.D.; Su, B.; Bettahar, N. Nickel-iron layered double hydroxide (LDH): Textural properties upon hydrothermal treatments and application on dye sorption. *J. Hazard. Mater.* **2009**, *165*, 206–217. [CrossRef]
60. Zhang, J.; De, W.; Cao, R.; Li, J. Hollow Fe_3O_4 nanospheres covered by phosphate-modified layered double hydroxides for the removal of uranium (VI) from water and soil. *Sep. Purif. Technol.* **2022**, *288*, 120688. [CrossRef]
61. Abellan, G.; Marti-gastaldo, C.; Ribera, A.; Coronado, E. Hybrid Materials Based on Magnetic Layered Double Hydroxides: A Molecular Perspective. *Accounts. Chem. Res.* **2015**, *48*, 1601–1611. [CrossRef] [PubMed]